use.[12,13] Patients who are able to stop smoking avoid the recurrence of the disease and amputation.[14] In addition, unlike those with atherosclerosis of the extremities, these patients rarely show involvement of visceral vessels and do not appear to be at an increased risk of stroke or myocardial infarction. The mortality rates are thus not higher than those of age- and sex-matched populations.[15,16] It is entirely possible that the high rate of adverse events observed in our patients may have been directly related to BM-MNC transplantation rather than to the progression of the disease itself.

Patient 4 suddenly died at 20 months after transplantation at the age of 30 years. The deaths of patients receiving BM-MNC transplantation were previously reported in the TACT study, in which 2 of 25 patients died of acute myocardial infarction within 24 weeks after transplantation.[11] The patients' backgrounds in the TACT study, in terms of age and comorbidity, may have been totally different from those of our study, in which only patients with thromboangiitis obliterans were recruited. As mentioned above, in patients with thromboangiitis obliterans, coronary involvement is rare, and they usually do very well as long as they discontinue smoking.[12–16] Patient 4 had no risk factors for atherosclerosis and stopped smoking before BM-MNC transplantation. Furthermore, ^{201}thallium scintigraphy performed before transplantation documented no sign of myocardial ischemia. Considering the patient's background and the natural course of the disease,[12–16] the possibility that his death was related to BM-MNC transplantation cannot be excluded. In this regard, several studies have suggested the possible role of BM-MNCs in atherogenesis. A recent report by Silvestre et al,[17] for example, demonstrated that the transplantation of BM-MNCs into ischemic limbs of apolipoprotein E–knockout mice led to a significant increase in atherosclerotic plaque size at a distant site. More recently, George et al[18] have also shown that an intravenous injection of bone marrow cells into apolipoprotein E–knockout mice results in an increase in atherosclerotic lesion size, whereas an injection of endothelial progenitor cells influences plaque stability. These reports indicate that attempts to enhance neovascularization by using BM-MNCs could also enhance unwanted plaque growth and instability, thus suggesting the possibility that our young patient died of an acute coronary event due to accelerated atherogenesis after BM-MNC transplantation.

We also encountered the development of an arteriovenous shunt, which could be a potential consequence of BM-MNC transplantation. Indeed, concerns have been raised about the potential adverse effects of cell transplantation, ie, unregulated differentiation and proliferation. Wakitani et al[19] reported that teratoma formation could occur after embryonic stem cell transplantation. Yoon et al[20] documented intramyocardial calcification after the transplantation of bone marrow cells in rats. Our observations may provide another cautionary example of unregulated differentiation and proliferation. Although the arteriovenous shunt in our case was self-limited, it may represent unwanted angiogenesis; thus, careful monitoring is warranted for future patients who receive BM-MNC transplantation.

Worsening or recurrence of ischemic symptoms was observed in 3 patients. The short-term outcome at 1 month was poor in these patients except in the patient with an arteriovenous shunt. The improvement in rest pain was not substantial in 1 patient. Healing of the skin ulcer was incomplete in another. It is anticipated that a poor response 1 month after BM-MNC transplantation could result in a poor long-term outcome. It is important to note that, in the latter patient with incomplete healing of the skin ulcer, the angiographic improvement of the collateral network at 1 month remained unchanged at 5 months when worsening of the skin ulcer was observed. It is suggested that the temporal sequence of improvement in ischemic limb status does not necessarily parallel the temporal evolution of collateral development.

Conclusions

In this unblinded and uncontrolled pilot study, long-term adverse events after BM-MNC transplantation, including death and unfavorable angiogenesis, were observed in half of the patients with thromboangiitis obliterans. Given the current incomplete knowledge of the safety and efficacy of this strategy, careful long-term monitoring is required for future patients receiving BM-MNC transplantation.

Sources of Funding

This work was supported by Health and Labor Sciences Research Grants (H16-009, H16-017, H17-009), by Ministry of Health, Labor and Welfare Research Grants for Cardiovascular Disease (16C-6, 18C-4), and by grants from the New Energy and Industrial Technology Development Organization and the Japan Cardiovascular Research Foundation.

Disclosures

None.

References

1. Belch JJ, Topol EJ, Agnelli G. Critical issues in peripheral arterial disease detection and management: a call to action. *Arch Intern Med*. 2003;28: 884–892.
2. Dormandy JA, Rutherford RB. Management of peripheral artery disease (PAD). TASC Working Group. TransAtlantic InterSociety Consensus (TASC). *J Vasc Surg*. 2000;31:S1–S296.
3. Isner JM, Rosenfield K. Redefining the treatment of peripheral artery disease. *Circulation*. 1993;88:1534–1557.
4. Takeshita S, Zheng LP, Brogi E, Kearney M, Pu LQ, Bunting S, Ferrara N, Symes JF, Isner JM. Therapeutic angiogenesis: a single intraarterial bolus of vascular endothelial growth factor augments revascularization in a rabbit ischemic hind limb model. *J Clin Invest*. 1994;93:662–670.
5. Isner J, Asahara T. Angiogenesis and vasculogenesis as therapeutic strategies for postnatal neovascularization. *J Clin Invest*. 1999;103: 1231–1236.
6. Asahara T, Murohara T, Sullivan A, Silver M, van der Zee R, Li T, Witzenbichler B, Schatteman G, Isner JM. Isolation of putative progenitor cells for angiogenesis. *Science*. 1997;275:964–967.
7. Asahara T, Masuda H, Takahashi T, Kalka C, Pastore C, Silver M, Kearney M, Magner M, Isner JM. Bone marrow origin of endothelial progenitor cells responsible for postnatal vasculogenesis in physiological and pathological neovascularization. *Circ Res*. 1999;85:221–228.
8. Shi Q, Rafii S, Wu M. Evidence for circulating bone marrow–derived endothelial cells. *Blood*. 1998;92:362–367.
9. Kalka C, Masuda H, Takahashi T, Kalka-Moll WM, Silver M, Kearney M, Li T, Isner JM, Asahara T. Transplantation of ex vivo expanded endothelial progenitor cells for therapeutic neovascularization. *Proc Natl Acad Sci U S A*. 2000;97:3423–3427.
10. Shintani S, Murohara T, Ikeda H, Ueno T, Sasaki K, Duan J, Imaizumi T. Augmentation of postnatal neovascularization with autologous bone marrow transplantation. *Circulation*. 2001;103:897–903.
11. Tateishi-Yuyama E, Matsubara H, Murohara T, Ikeda U, Shintani S, Masaki H, Amano K, Kishimoto Y, Yoshimoto K, Akashi H, Shimada K,

Iwasaka T, Imaizumi T. Therapeutic angiogenesis for patients with limb ischemia by autologous transplantation of bone marrow cells: a pilot study and a randomized controlled trial. *Lancet*. 2002;360:427–435.
12. Olin JW. Thromboangiitis obliterans (Buerger's disease). *N Engl J Med*. 2000;343:864–869.
13. Olin JW, Young JR, Graor RA, Ruschhaupt WF, Bartholomew JR. The changing clinical spectrum of thromboangiitis obliterans (Buerger's disease). *Circulation*. 1990;82(5 Suppl):IV3–IV8.
14. Matsushita M, Shionoya S, Matsumoto T. Urinary cotinine measurement in patients with Buerger's diseases: effects of active and passive smoking on the disease process. *J Vasc Surg*. 1991;14:53–58.
15. Szuba A, Cooke JP. Thromboangiitis obliterans: an update on Buerger's disease. *West J Med*. 1998;168:225–260.
16. Mills JL, Taylor LMJ, Porter JM. Buerger's disease in the modern era. *Am J Surg*. 1987;154:123–129.
17. Silvestre J-S, Gojova A, Brun V, Potteaux S, Esposito B, Duriez M, Clergue M, Le Ricousse-Roussanne S, Barateau V, Merval R, Groux H, Tobelem G, Levy B, Tedgui A, Mallat Z. Transplantation of bone marrow–derived mononuclear cells in ischemic apolipoprotein E–knockout mice accelerates atherosclerosis without altering plaque composition. *Circulation*. 2003;108:2839–2842.
18. George J, Afek A, Abashidze A, Shmilovich H, Deutsch V, Kopolovich J, Miller H, Keren G. Transfer of endothelial progenitor and bone marrow cells influences atherosclerotic plaque size and composition in apolipoprotein E knockout mice. *Arterioscler Thromb Vasc Biol*. 2005;25:2636–2641.
19. Wakitani S, Takaoka K, Hattori T, Miyazawa N, Iwanaga T, Takeda S, Watanabe TK, Tanigami A. Embryonic stem cells injected into the mouse knee joint form teratomas and subsequently destroy the joint. *Rheumatology (Oxford)*. 2003;42:162–165.
20. Yoon Y, Park J, Tkebuchava T, Luedeman C, Losordo D. Unexpected severe calcification after transplantation of bone marrow cells in acute myocardial infarction. *Circulation*. 2004;109:3154–3157.

CLINICAL PERSPECTIVE

The favorable short-term outcome of bone marrow mononuclear cell transplantation (BM-MNC) transplantation has been established in patients with critical limb ischemia. However, the long-term outcome of this treatment strategy has not been determined yet. In our case series, we documented that long-term adverse events, including death and unfavorable angiogenesis, were observed in 4 of 8 patients receiving BM-MNC transplantation. The first patient suffered sudden death at 20 months after transplantation at 30 years of age. The second patient with incomplete healing of a skin ulcer showed worsening of the lesion at 4 months. The third patient had worsening of rest pain at 8 months. The last patient developed an arteriovenous shunt in the foot at 7 months, which spontaneously regressed by 1 year. Given the current incomplete knowledge on the safety and efficacy of this strategy, it is suggested that careful long-term monitoring is required in patients receiving BM-MNC transplantation. To our knowledge, this is the first report on the long-term outcome of transplantation of BM-MNCs for critical limb ischemia, and the first that documents the development of unfavorable angiogenesis and sudden death after therapeutic angiogenesis.

Japanese Journal of Applied Physics
Vol. 45, No. 6A, 2006, pp. 5301–5306

X-ray Spectra from Weakly Ionized Linear Copper Plasma

Eiichi SATO, Yasuomi HAYASHI, Rudolf GERMER[1], Etsuro TANAKA[2], Hidezo MORI[3], Toshiaki KAWAI[4], Takashi INOUE[5], Akira OGAWA[5], Shigehiro SATO[6], Kazuyoshi TAKAYAMA[7] and Jun ONAGAWA[8]

Department of Physics, Iwate Medical University, 3-16-1 Honchodori, Morioka 020-0015, Japan
[1]*ITP, FHTW FB1 and TU-Berlin, Blankenhainer Str. 9, D 12249 Berlin, Germany*
[2]*Department of Nutritional Science, Faculty of Applied Bio-science, Tokyo University of Agriculture, 1-1-1 Sakuragaoka, Setagaya-ku, Tokyo 156-8502, Japan*
[3]*Department of Cardiac Physiology, National Cardiovascular Center Research Institute, 5-7-1 Fujishirodai, Suita, Osaka 565-8565, Japan*
[4]*Electron Tube Division #2, Hamamatsu Photonics K.K., 314-5 Shimokanzo, Iwata, Shizuoka 438-0193, Japan*
[5]*Department of Neurosurgery, School of Medicine, Iwate Medical University, 19-1 Uchimaru, Morioka 020-8505, Japan*
[6]*Department of Microbiology, School of Medicine, Iwate Medical University, 19-1 Uchimaru, Morioka 020-8505, Japan*
[7]*Shock Wave Research Center, Institute of Fluid Science, Tohoku University, 2-1-1 Katahira, Sendai 980-8577, Japan*
[8]*Department of Applied Physics and Informatics, Faculty of Engineering, Tohoku Gakuin University, 1-13-1 Chuo, Tagajo, Miyagi 985-8537, Japan*

(Received November 20, 2005; accepted April 5, 2006; published online June 8, 2006)

In the plasma flash X-ray generator, a 200 nF condenser is charged up to 50 kV by a power supply, and flash X-rays are produced by the discharging. The X-ray tube is a demountable triode with a trigger electrode, and the turbomolecular pump evacuates air from the tube with a pressure of approximately 1 mPa. Target evaporation leads to the formation of weakly ionized linear plasma, consisting of copper ions and electrons, around the fine target, and intense Kα lines are left using a 10-μm-thick nickel filter. At a charging voltage of 50 kV, the maximum tube voltage was almost equal to the charging voltage of the main condenser, and the peak current was about 16 kA. The K-series characteristic X-rays were clean and intense, and higher harmonic X-rays were observed. The X-ray pulse widths were approximately 300 ns, and the time-integrated X-ray intensity had a value of approximately 1.5 mGy per pulse at 1.0 m from the X-ray source with a charging voltage of 50 kV. [DOI: 10.1143/JJAP.45.5301]

KEYWORDS: linear plasma, X-ray spectra, K-series characteristic X-rays, bremsstrahlung X-rays, higher harmonic X-rays

1. Introduction

In order to produce X-ray lasers, several different methods have been developed, and a discharge capillary[1–3] is very useful to increase the laser pulse energy with increases in the capillary length. However, it is difficult to increase the laser photon energy to 10 keV or beyond.

Using monochrocollimators, synchrotrons produce monochromatic parallel beams, which are fairly similar to monochromatic parallel laser beams, and the beams have been applied to various research project including phase-contrast radiography[4,5] and enhanced K-edge angiography.[6,7] Because there are no X-ray resonators in the high-photon-energy region, new methods for increasing coherence will be desired in the future.

To apply flash X-ray generators to biomedicine, several different generators[8–13] have been developed, and plasma X-ray generators[14–17] are useful for producing clean characteristic X-rays in the low-photon-energy region of less than 10 keV. By forming weakly ionized linear plasma using rod targets, intense K-series characteristic X-rays are observed from the axial direction of the linear plasmas of nickel and copper, since the bremsstrahlung X-rays are absorbed effectively by the linear plasma. We are therefore very interested in the X-ray spectra produced by increasing the charging voltage in the high photon energy region beyond Kβ energies.

In this paper, we describe a recent table-top plasma flash X-ray generator utilizing a rod target triode, used to perform a preliminary experiment for generating clean K-series characteristic X-rays and their higher harmonic hard X-rays by forming a linear copper plasma cloud around a fine target.

2. Generator

Figure 1 shows a block diagram of the high-intensity plasma flash X-ray generator. This generator consists of the following essential components: a high-voltage power supply, a high-voltage condenser with a capacity of approximately 200 nF, a turbomolecular pump, a krytron pulse generator as a trigger device, and a flash X-ray tube. The high-voltage main condenser is charged to 50 kV by the power supply, and electric charges in the condenser are discharged to the tube after triggering the cathode electrode with the trigger device. The plasma flash X-rays are then produced.

The X-ray tube is a demountable cold-cathode triode that is connected to the turbomolecular pump with a pressure of approximately 1 mPa. This tube consists of the following major parts: a hollow cylindrical carbon cathode with a bore diameter of 10.0 mm, a brass focusing electrode, a trigger electrode made from copper wire, a stainless steel vacuum chamber, a nylon insulator, a poly(ethylene terephthalate) (Mylar) X-ray window 0.25 mm in thickness, and a rod-shaped copper target 3.0 mm in diameter with a tip angle of 60°. The distance between the target and cathode electrodes is approximately 20 mm, and the trigger electrode is set in the cathode electrode. As electron beams from the cathode electrode are roughly converged to the target by the focusing electrode, evaporation leads to the formation of a weakly ionized linear plasma,[18] consisting of copper ions and electrons, around the fine target.

In the linear plasma, bremsstrahlung photons with energies higher than the K-absorption edge are effectively absorbed and are converted into fluorescent X-rays. The plasma then transmits the fluorescent rays easily, and bremsstrahlung rays with energies lower than the K-edge

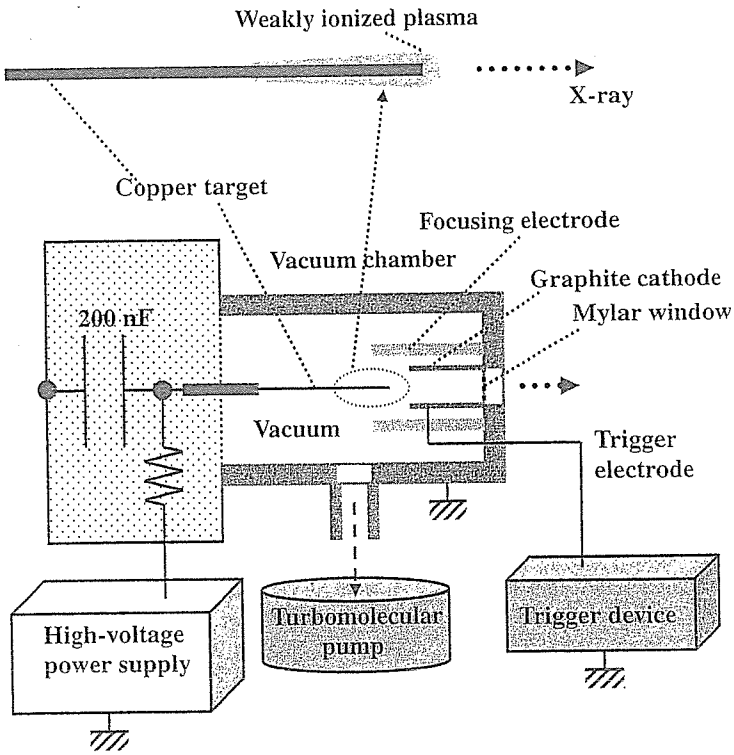

Fig. 1. Block diagram including the electric circuit of the plasma flash X-ray generator.

are also absorbed by the plasma. In addition, because bremsstrahlung rays are not emitted in the opposite direction to that of electron trajectory, intense characteristic X-rays are generated from the plasma-axial direction.

3. Characteristics

3.1 Tube voltage and current

Tube voltage and current were measured by a high-voltage divider with an input impedance of 1 GΩ and a current transformer, respectively. The withstand voltage of the divider is approximately 60 kV, and the measurable current of the transformer ranges from 1 A to 100 kA. Figure 2 shows the time relation between the tube voltage and current. At the indicated charging voltages, they roughly displayed damped oscillations. When the charging voltage was increased, both the maximum tube voltage and current increased. At a charging voltage of 50 kV, the maximum tube voltage was almost equal to the charging voltage of the main condenser, and the maximum tube current was approximately 16 kA.

3.2 X-ray output

X-ray output pulse was detected using a combination of a plastic scintillator and a photomultiplier (Fig. 3). The X-ray pulse height substantially increased with corresponding increases in the charging voltage. The rise time increased with increasing the voltage because the K-series characteristic X-rays were produced with tube voltages beyond the critical excitation voltage of 8.9 kV. The X-ray pulse widths were about 300 ns, and the time-integrated X-ray intensity per pulse measured by a thermoluminescence dosimeter (Kyokko TLD Reader 1500 having MSO-S elements without energy compensation) had a value of approximately 1.5 mGy at 1.0 m from the X-ray source with a charging voltage of 50 kV. The TLD reader has a wide measurable range of from 1 μSv to 100 Sv.

3.3 X-ray source

In order to roughly observe images of the plasma X-ray source in the detector plane, we employed a pinhole camera with a hole diameter of 100 μm without using a filter (Fig. 4). When the charging voltage was increased, the plasma X-ray source grew, and both spot dimension and intensity increased. Because the X-ray intensity is the highest at the center of the spot, both the dimension and intensity decreased according to both increases in the thickness of a filter for absorbing X-rays and decreases in the pinhole diameter.

3.4 X-ray spectra

X-ray spectra from the plasma source were measured by a transmission-type spectrometer with a lithium fluoride curved crystal 0.5 mm in thickness. The spectra were taken by a computed radiography (CR) system[19] (Konica Minolta, Regius 150) with a wide dynamic range beyond five figures for measuring X-ray intensity, and relative X-ray intensity was calculated from Dicom digital data. Subsequently, the relative X-ray intensity as a function of the data was calibrated using a conventional X-ray generator, and we confirmed that the intensity was proportional to the exposure time. Figure 5 shows measured spectra from the copper target at the indicated conditions. In fact, we observed clean K lines, and Kα lines were left by absorbing Kβ lines using a 10-μm-thick nickel filter. When the charging voltage was increased, the characteristic X-ray intensity substantially increased. In particular, we confirmed the irradiation of

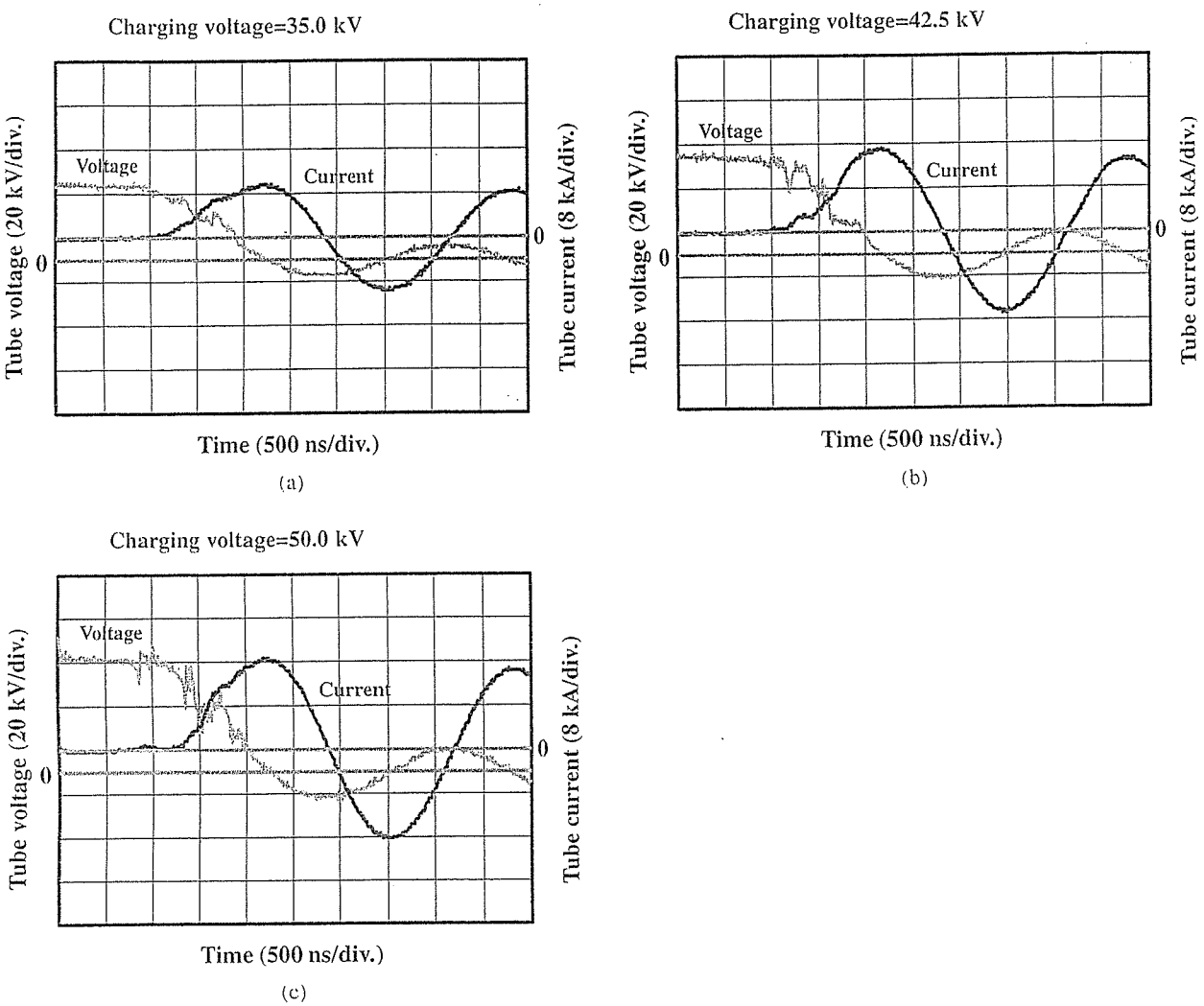

Fig. 2. Tube voltages and currents with a charging voltage of (a) 35.0, (b) 42.5, and (b) 50.0 kV.

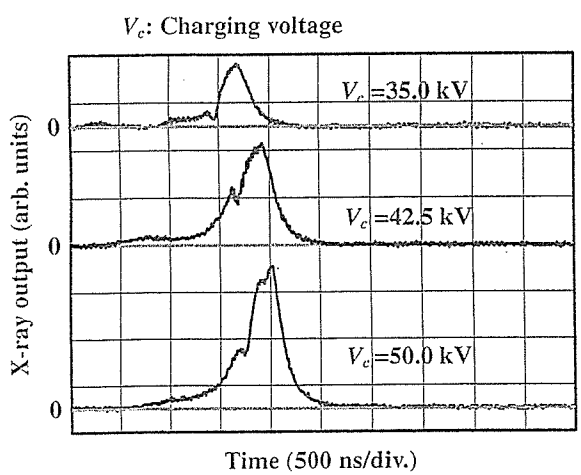

Fig. 3. X-ray outputs at the indicated conditions.

the second and fourth harmonic X-rays of the fundamental K-series characteristic X-rays from copper target. The X-ray intensities of the harmonics increased with increases in the charging voltage, and the harmonic bremsstrahlung rays survived due to the X-ray resonation in the plasma.

4. Radiography

The plasma radiography was performed by the CR system using the filter. The charging voltage and the distance between the X-ray source and imaging plate were 50 kV and 1.2 m, respectively. First, rough measurements of spatial resolution were made using wires. Figure 6 shows radiograms of tungsten wires coiled around pipes made of poly(methyl methacrylate) (PMMA). Although the image contrast decreased somewhat with decreases in the wire diameter, due to blurring of the image caused by the sampling pitch of 87.5 μm, a 50-μm-diameter wire could be observed.

Figure 7 shows a radiogram of plastic bullets falling into a polypropylene beaker from a plastic test tube. Because the X-ray duration was about 0.5 μs, the stop-motion image of bullets could be obtained. Next, a radiogram of a vertebra is shown in Fig. 8, and fine structures in the vertebra were observed. Finally, Fig. 9 shows an angiogram of a rabbit ear; iodine-based microspheres of 15 μm in diameter were used, and fine blood vessels of about 100 μm were visible.

5. Conclusions and Outlook

We obtained fairly intense and clean K lines from a weakly ionized linear copper plasma, and Kα lines were left

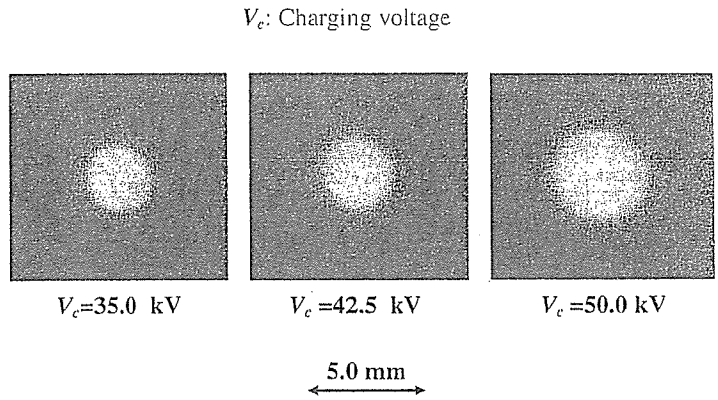

Fig. 4. Images of the plasma X-ray source.

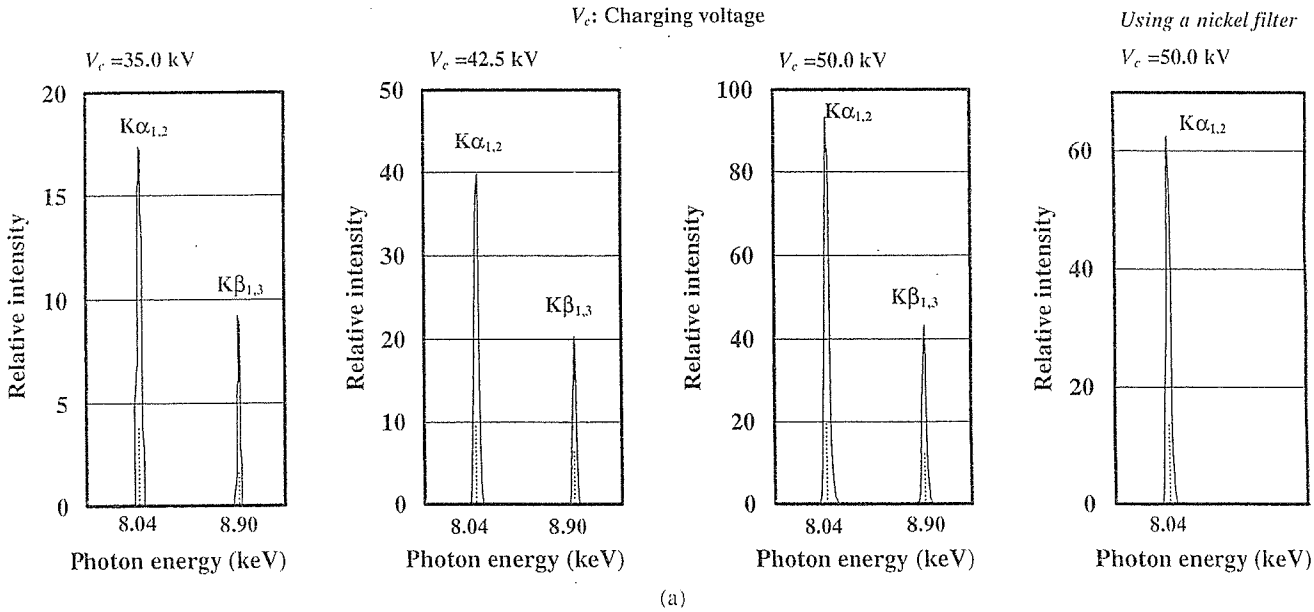

(a)

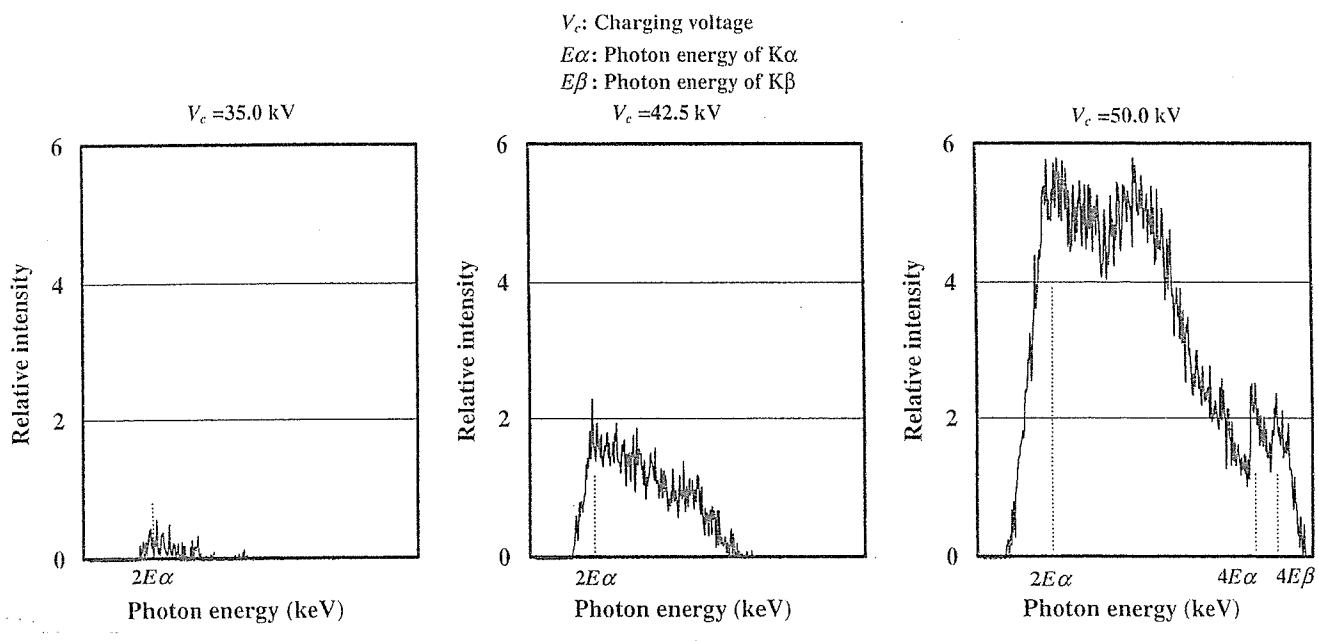

(b)

Fig. 5. X-ray spectra from weakly ionized copper plasma at the indicated conditions. (a) characteristic X-rays and (b) higher harmonic X-rays.

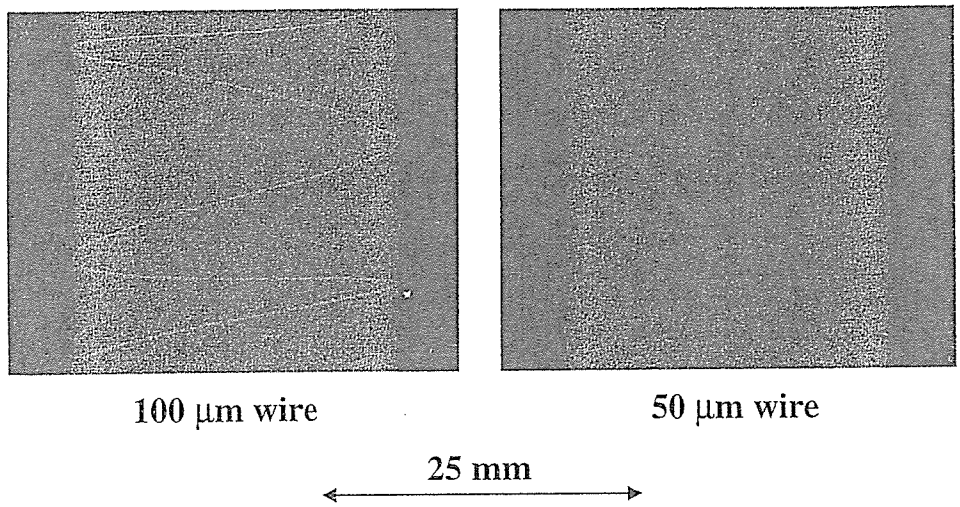

Fig. 6. Radiograms of tungsten wires coiled around PMMA pipes.

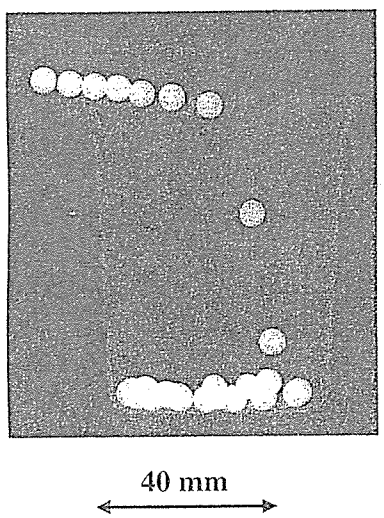

Fig. 7. Radiogram of plastic bullets falling into polypropylene beaker from a plastic test tube.

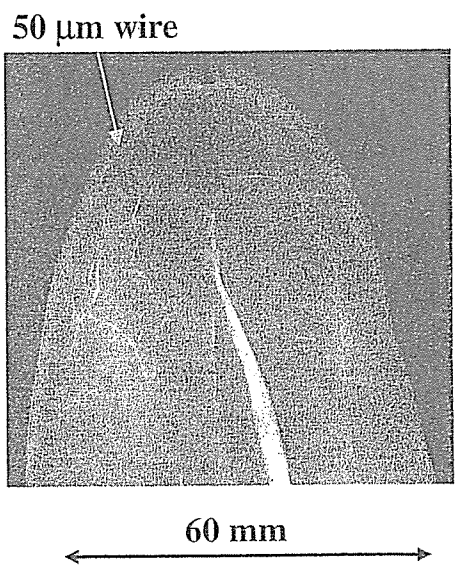

Fig. 9. Angiogram of a rabbit ear.

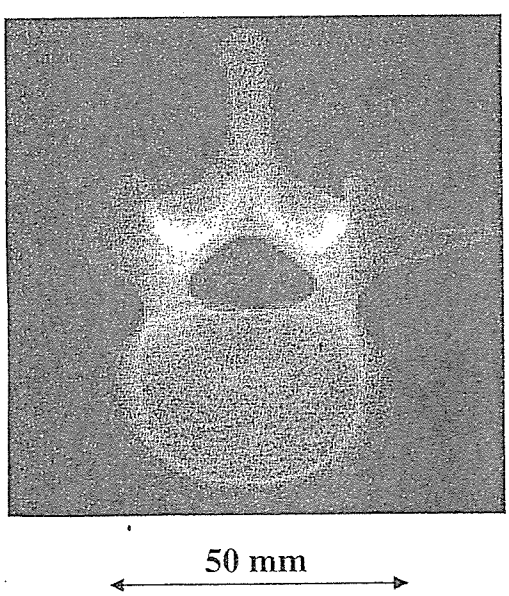

Fig. 8. Radiogram of a vertebra.

by the nickel filter. Both the characteristic and the harmonic X-ray intensities substantially increased with increasing the charging voltage.

In cases where weakly ionized linear plasma is employed, intense and clean K-series characteristic X-rays can be obtained. However, it is not easy to produce high-photon-energy K-series characteristic X-rays because the linear plasma transmits high-photon-energy bremsstrahlung X-rays; the effective thickness of a monochromatic metal filter increases with increases in the atomic number. Therefore, high-photon-energy plasma flash X-ray generators utilizing the angle dependence of bremsstrahlung X-rays are very useful to produce K photons of molybdenum, silver, cerium, tantalum, and tungsten. In particular, Kα rays of tantalum and tungsten are useful for performing enhanced K-edge angiography using gadolinium contrast media, and cerium K rays can be employed to perform iodine K-edge angiography.

In this research, we obtained sufficient characteristic X-ray intensity per pulse for CR radiography, and the

generator produced number of characteristic K photons was approximately 1×10^8 photons/cm^2 at 1.0 m per pulse. In addition, we are very interested in producing steady-state clean K rays and their higher harmonic hard X-rays using a similar tube.

Acknowledgments

This work was supported by Grants-in-Aid for Scientific Research (13470154, 13877114, 16591181, and 16591222) and Advanced Medical Scientific Research from MECSST, Health and Labor Sciences Research Grants (RAMT-nano-001, RHGTEFB-genome-005 and RHGTEFB-saisei-003), Grants from The Keiryo Research Foundation, The Promotion and Mutual Aid Corporation for Private Schools of Japan, Japan Science and Technology Agency (JST), and the New Energy and Industrial Technology Development Organization (NEDO, Industrial Technology Research Grant Program in '03).

1) J. J. Rocca, V. Shlyaptsev, F. G. Tomasel, O. D. Cortazar, D. Hartshorn and J. L. A. Chilla: Phys. Rev. Lett. **73** (1994) 2192.
2) C. D. Macchietto, B. R. Benware and J. J. Rocca: Opt. Lett. **24** (1999) 1115.
3) J. J. G. Rocca, J. L. A. Chilla, S. Sakadzic, A. Rahman, J. Filevich, E. Jankowska, E. C. Hammarsten, B. M. Luther, H. C. Kapteyn, M. Murnane and V. N. Shlyapsev: Proc. SPIE **4505** (2001) 1.
4) A. Momose, T. Takeda, Y. Itai and K. Hirano: Nat. Med. **2** (1996) 473.
5) M. Ando, A. Maksimenko, H. Sugiyama, W. Pattanasiriwisawa, K. Hyodo and C. Uyama: Jpn. J. Appl. Phys. **41** (2002) L1016.
6) H. Mori *et al.*: Radiology **201** (1996) 173.
7) K. Hyodo, M. Ando, Y. Oku, S. Yamamoto, T. Takeda, Y. Itai, S. Ohtsuka, Y. Sugishita and J. Tada: J. Synchrotron Radiat. **5** (1998) 1123.
8) E. Sato, S. Kimura, S. Kawasaki, H. Isobe, K. Takahashi, Y. Tamakawa and T. Yanagisawa: Rev. Sci. Instrum. **61** (1990) 2343.
9) K. Takahashi, E. Sato, M. Sagae, T. Oizumi, Y. Tamakawa and T. Yanagisawa: Jpn. J. Appl. Phys. **33** (1994) 4146.
10) E. Sato, K. Takahashi, M. Sagae, S. Kimura, T. Oizumi, Y. Hayasi, Y. Tamakawa and T. Yanagisawa: Med. Biol. Eng. Comput. **32** (1994) 289.
11) E. Sato, M. Sagae, K. Takahashi, A. Shikoda, T. Oizumi, Y. Hayasi, Y. Tamakawa and T. Yanagisawa: Med. Biol. Eng. Comput. **32** (1994) 295.
12) E. Sato, M. Sagae, E. Tanaka, Y. Hayasi, R. Germer, H. Mori, T. Kawai, T. Ichimaru, S. Sato, K. Takayama and H. Ido: Jpn. J. Appl. Phys. **43** (2004) 7324.
13) E. Sato, E. Tanaka, H. Mori, T. Kawai, T. Ichimaru, S. Sato, K. Takayama and H. Ido: Med. Phys. **32** (2005) 49.
14) E. Sato, Y. Hayasi, R. Germer, E. Tanaka, H. Mori, T. Kawai, H. Obara, T. Ichimaru, K. Takayama and H. Ido: Jpn. J. Med. Phys. **23** (2003) 123.
15) E. Sato, Y. Hayasi, R. Germer, E. Tanaka, H. Mori, T. Kawai, T. Ichimaru, K. Takayama and H. Ido: Rev. Sci. Instrum. **74** (2003) 5236.
16) E. Sato, Y. Hayasi, R. Germer, E. Tanaka, H. Mori, T. Kawai, T. Ichimaru, S. Sato, K. Takayama and H. Ido: J. Electron Spectrosc. Relat. Phenom. C **137–140** (2004) 713.
17) E. Sato, E. Tanaka, H. Mori, T. Kawai, S. Sato and K. Takayama: Opt. Eng. **44** (2005) 049002.
18) E. Sato, M. Sagae, K. Takahashi, T. Ichimaru, W. Aiba, S. Kumagai, Y. Hayasi, H. Ido, K. Sakamaki, K. Takayama and Y. Tamakawa: Proc. SPIE **3336** (1998) 75.
19) E. Sato, K. Sato and Y. Tamakawa: Ann. Rep. Iwate Med. Univ. Sch. Lib. Arts Sci. **35** (2000) 13.

Available online at www.sciencedirect.com
ScienceDirect
Radiation Physics and Chemistry 75 (2006) 1812–1818
Radiation Physics and Chemistry
www.elsevier.com/locate/radphyschem

Preliminary study for producing higher harmonic hard X-rays from weakly ionized nickel plasma

Eiichi Sato[a,*], Yasuomi Hayasi[a], Etsuro Tanaka[b], Hidezo Mori[c], Toshiaki Kawai[d], Takashi Inoue[e], Akira Ogawa[e], Shigehiro Sato[f], Kazuyoshi Takayama[g], Jun Onagawa[h], Hideaki Ido[h]

[a]*Department of Physics, Iwate Medical University, 3-16-1 Honchodori, Morioka 020-0015, Japan*
[b]*Department of Nutritional Science, Faculty of Applied Bio-science, Tokyo University of Agriculture, 1-1-1 Sakuragaoka, Setagaya-ku 156-8502, Japan*
[c]*Department of Cardiac Physiology, National Cardiovascular Center Research Institute, 5-7-1 Fujishirodai, Suita, Osaka 565-8565, Japan*
[d]*Electron Tube Division #2, Hamamatsu Photonics K. K., 314-5 Shimokanzo, Iwata 438-0193, Japan*
[e]*Department of Neurosurgery, School of Medicine, Iwate Medical Universichimaru, Morioka 020-8505, Japan*
[f]*Department of Microbiology, School of Medicine, Iwate Medical University, 19-1 Uchimaru, Morioka 020-8505, Japan*
[g]*Shock Wave Research Center, Institute of Fluid Science, Tohoku University, 2-1-1 Katahira, Sendai 980-8577, Japan*
[h]*Department of Applied Physics and Informatics, Faculty of Engineering, Tohoku Gakuin University, 1-13-1 Chuo, Tagajo 985-8537, Japan*

Accepted 23 November 2005

Abstract

In the plasma flash X-ray generator, a 200 nF condenser is charged up to 50 kV by a power supply, and flash X-rays are produced by the discharging. The X-ray tube is a demountable triode with a trigger electrode, and the turbomolecular pump evacuates air from the tube with a pressure of approximately 1 mPa. Target evaporation leads to the formation of weakly ionized linear plasma, consisting of nickel ions and electrons, around the fine target, and intense Kα lines are left using a 15-μm-thick cobalt filter. At a charging voltage of 50 kV, the maximum tube voltage was almost equal to the charging voltage of the main condenser, and the peak current was about 18 kA. The K-series characteristic X-rays were clean and intense, and higher harmonic X-rays were observed. The X-ray pulse widths were approximately 300 ns, and the time-integrated X-ray intensity had a value of approximately 1.0 mGy at 1.0 m from the X-ray source with a charging voltage of 50 kV.

PACS: 52.80.Vp; 52.90.+z; 87.59.Bh; 87.64.Gb

Keywords: Weakly ionized linear plasma; K-series characteristic X-rays; Clean characteristic X-rays; Higher harmonic hard X-rays

1. Introduction

In conjunction with single crystals, synchrotrons produce monochromatic parallel beams, which are fairly similar to monochromatic parallel laser beams, and the

*Corresponding author.
E-mail address: dresato@iwate-med.ac.jp (E. Sato).

0969-806X/$ - see front matter © 2006 Elsevier Ltd. All rights reserved.
doi:10.1016/j.radphyschem.2005.11.012

beams have been applied to enhanced K-edge angiography (Thompson et al., 1992; Mori et al., 1996; Hyodo et al., 1998), phase-contrast radiography (Davis et al., 1995; Momose et al., 1996; Ando et al., 2002), and crystallography. Therefore, the production of coherent hard X-ray lasers for various research projects, including biomedical applications, has long been wished for.

Recently, soft X-ray lasers have been produced by a gas-discharge capillary (Rocca et al., 1994, 1996; Macchietto et al., 1999), and the laser pulse energy substantially increased in proportion to the capillary length. These kinds of fast discharges can generate hot and dense plasma columns with aspect ratios approaching 1000:1. However, it is difficult to increase the laser photon energy to 10 keV or beyond. Because there are no X-ray resonators in the high-photon-energy region, new methods for increasing coherence will be desired in the future.

To apply flash X-ray generators to biomedicine, several different generators have been developed (Germer, 1979; Sato et al., 1990, 1994a, b; Shikoda et al., 1994; Takahashi et al., 1994), and plasma X-ray generators (Sato et al., 2003a, b, 2004a–c, 2005a–c) are useful for producing clean characteristic X-rays in the low-photon-energy region of less than 20 keV. By forming weakly ionized linear plasma using rod targets, we confirmed irradiation of intense K-series characteristic X-rays from the axial direction of the linear plasmas of nickel, copper, and molybdenum, since the bremsstrahlung X-rays are absorbed effectively by the linear plasma; monochromatic clean Kα rays were produced using K-edge filters.

In this paper, we describe a recent plasma flash X-ray generator utilizing a rod target, used to perform a preliminary experiment for generating clean K-series characteristic X-rays and their higher harmonic hard X-rays by forming a plasma cloud around a fine target.

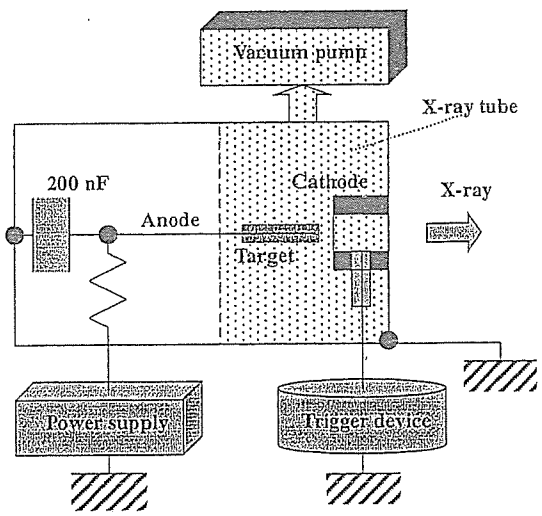

Fig. 1. Block diagram including electric circuit of the plasma flash X-ray generator.

2. Generator

Fig. 1 shows a block diagram of the high-intensity plasma flash X-ray generator. This generator consists of the following essential components: a high-voltage power supply, a high-voltage condenser with a capacity of approximately 200 nF, a turbomolecular pump, a krytron pulse generator as a trigger device, and a flash X-ray tube. The high-voltage main condenser is charged to 50 kV by the power supply, and electric charges in the condenser are discharged to the tube after triggering the cathode electrode with the trigger device. The plasma flash X-rays are then produced.

The schematic drawing of the plasma X-ray tube is illustrated in Fig. 2. The X-ray tube is a demountable

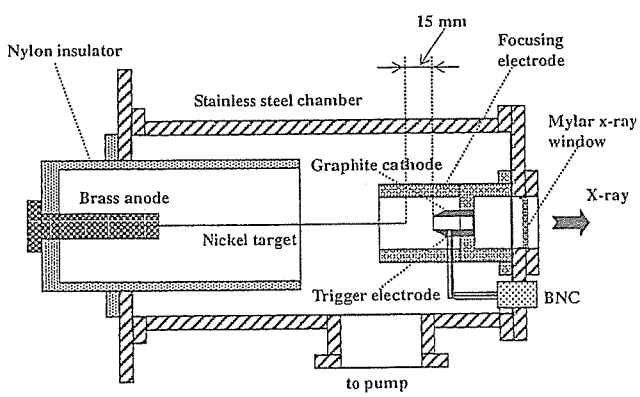

Fig. 2. Schematic drawing of the flash X-ray tube with a rod nickel target.

cold-cathode triode that is connected to the turbomolecular pump with a pressure of approximately 1 mPa. This tube consists of the following major parts: a hollow cylindrical carbon cathode with a bore diameter of 10.0 mm, a brass focusing electrode, a trigger electrode made from copper wire, a stainless steel vacuum chamber, a nylon insulator, a polyethylene terephthalate (Mylar) X-ray window 0.25 mm in thickness, and a rod-shaped nickel target 3.0 mm in diameter with a tip angle of 60°. The distance between the target and cathode electrodes is approximately 15 mm, and the trigger electrode is set in the cathode electrode. As electron beams from the cathode electrode are roughly converged to the target by the focusing electrode, evaporation leads to the formation of a weakly ionized linear plasma, consisting of nickel ions and electrons, around the fine target.

In the linear plasma, bremsstrahlung photons with energies higher than the K-absorption edge are effectively absorbed and are converted into fluorescent X-rays. The plasma then transmits the fluorescent rays easily, and bremsstrahlung rays with energies lower than the K-edge are also absorbed by the plasma. In addition, because bremsstrahlung rays are not emitted in the opposite direction to that of electron trajectory, intense characteristic X-rays are generated from the plasma-axial direction.

3. Characteristics

3.1. Tube voltage and current

Tube voltage and current were measured by a high-voltage divider with an input impedance of 1 GΩ and a current transformer, respectively. Fig. 3 shows the time relation between the tube voltage and current. At the indicated charging voltages, they roughly displayed damped oscillations. When the charging voltage was increased, both the maximum tube voltage and current increased. At a charging voltage of 50 kV, the maximum tube voltage was almost equal to the charging voltage of the main condenser, and the maximum tube current was approximately 18 kA.

3.2. X-ray output

X-ray output pulse was detected using a combination of a plastic scintillator and a photomultiplier (Fig. 4). The X-ray pulse height substantially increased with corresponding increases in the charging voltage. The X-ray pulse widths were about 300 ns, and the time-integrated X-ray intensity measured by a thermoluminescence dosimeter (Kyokko TLD Reader 1500 having MSO-S elements without energy compensation) had a value of about 1.0 mGy at 1.0 m from the X-ray source with a charging voltage of 50 kV.

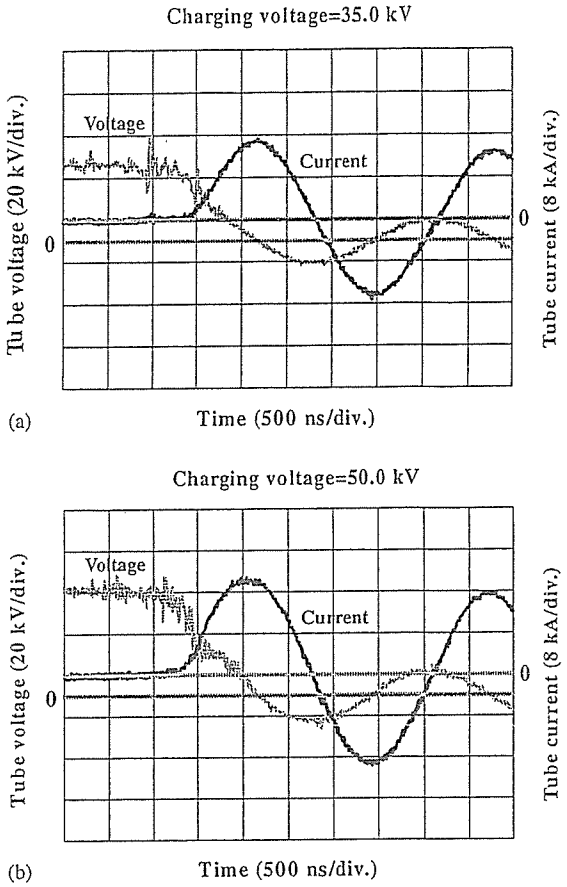

Fig. 3. Tube voltages and currents with a charging voltage of (a) 35.0 kV and (b) 50.0 kV.

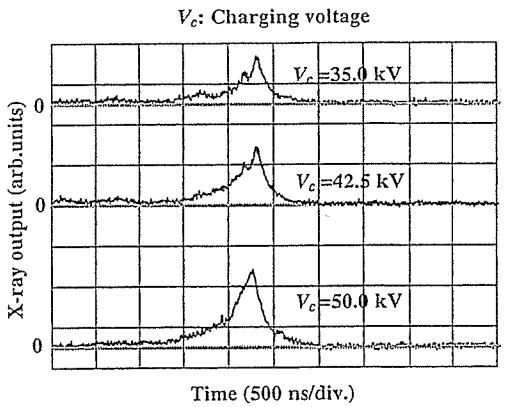

Fig. 4. X-ray outputs at the indicated conditions.

3.3. X-ray source

In order to roughly observe images of the plasma X-ray source in the detector plane, we employed a pinhole camera with a hole diameter of 100 μm (Fig. 5). When

the charging voltage was increased, the plasma X-ray source grew, and both spot dimension and intensity increased. Because the X-ray intensity is the highest at the center of the spot, both the dimension and intensity decreased according to both increases in the thickness of a filter for absorbing X-rays and decreases in the pinhole diameter.

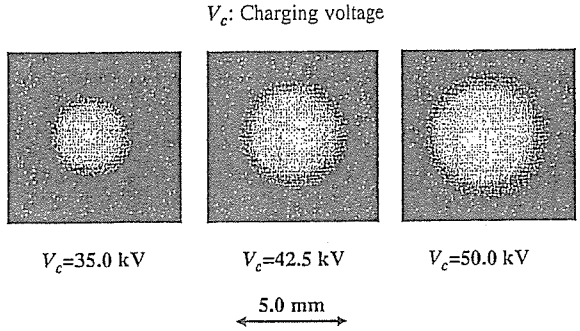

Fig. 5. Images of plasma X-ray source.

3.4. X-ray spectra

X-ray spectra from the plasma source were measured by a transmission-type spectrometer with a lithium fluoride curved crystal 0.5 mm in thickness. The spectra were taken by a computed radiography (CR) system (Sato et al., 2000) (Konica Minolta Regius 150) with a wide dynamic range, and relative X-ray intensity was calculated from Dicom digital data. Subsequently, the relative X-ray intensity as a function of the data was calibrated using a conventional X-ray generator, and we confirmed that the intensity was proportional to the

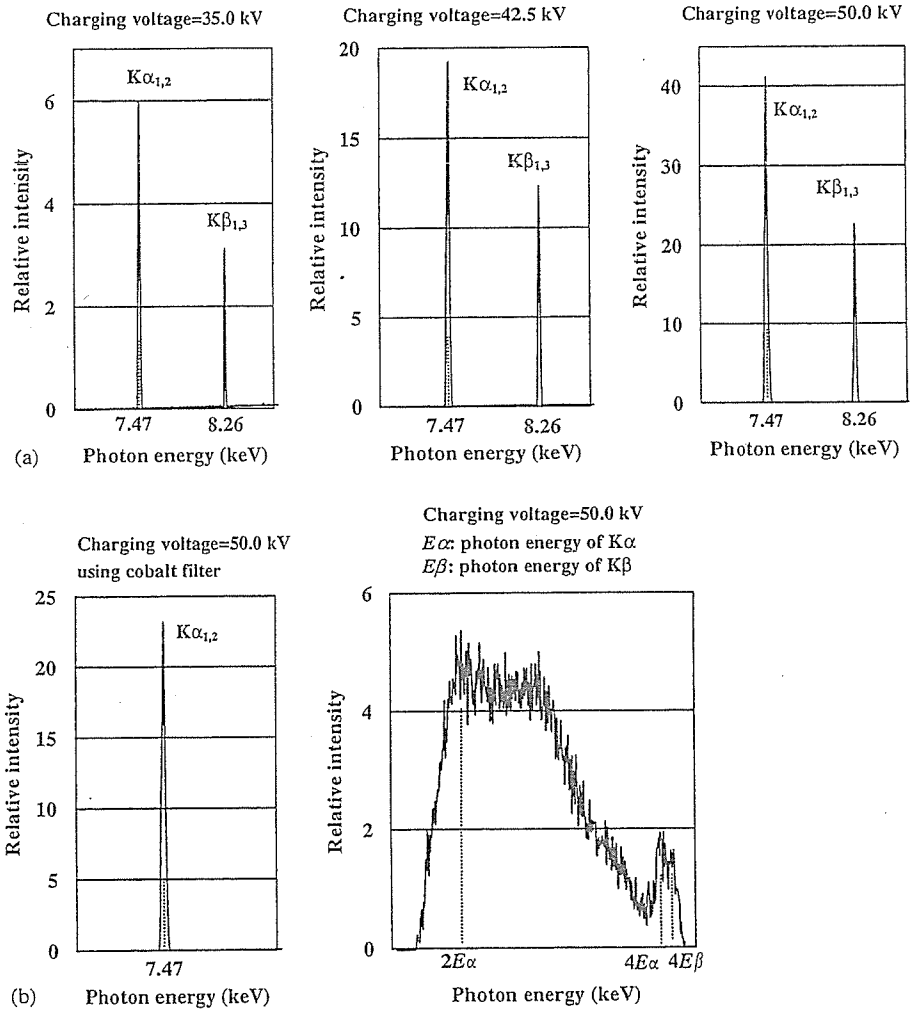

Fig. 6. X-ray spectra from weakly ionized nickel plasma at the indicated conditions. (a) Kα and Kβ rays and (b) Kα and higher harmonic rays.

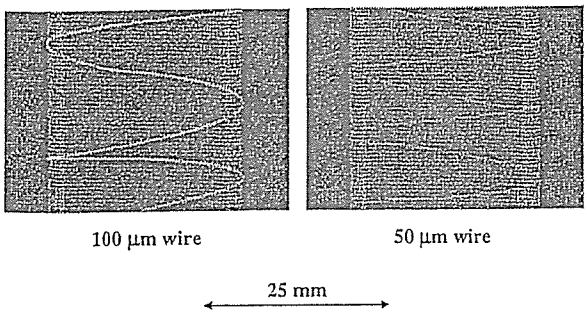

Fig. 7. Radiograms of tungsten wires coiled around PMMA pipes.

exposure time. Fig. 6 shows measured spectra from the copper target with a charging voltage of 50 kV. In fact, we observed clean K lines such as lasers, and Kα lines were left by absorbing Kβ lines using a 15-μm-thick cobalt filter. The characteristic X-ray intensity substantially increased with corresponding increases in the charging voltage, and higher harmonic hard X-rays were observed.

4. Radiography

The plasma radiography was performed by the CR system without using the filter. The charging voltage and the distance between the X-ray source and imaging plate were 50 kV and 1.2 m, respectively.

Firstly, rough measurements of spatial resolution were made using wires. Fig. 7 shows radiograms of tungsten wires coiled around pipes made of polymethyl methacrylate (PMMA). Although the image contrast decreased somewhat with decreases in the wire diameter, due to blurring of the image caused by the sampling pitch of 87.5 μm, a 50-μm-diameter wire could be observed.

Fig. 8 shows a radiogram of a vertebra, and fine structures in the vertebra were observed. Next, an image of plastic bullets falling into a polypropylene beaker from a plastic test tube is shown in Fig. 9. Because the X-ray duration was about 500 ns, the stop-motion image of bullets could be obtained.

5. Conclusions and outlook

Concerning the spectrum measurement, we obtained fairly intense and clean K lines from a weakly ionized linear plasma X-ray source, and Kα lines were left by absorbing Kβ lines using the cobalt filter. In particular, the higher harmonic X-rays were produced from the plasma. Because the X-ray intensities of the harmonics increased with increases in the charging voltage, the

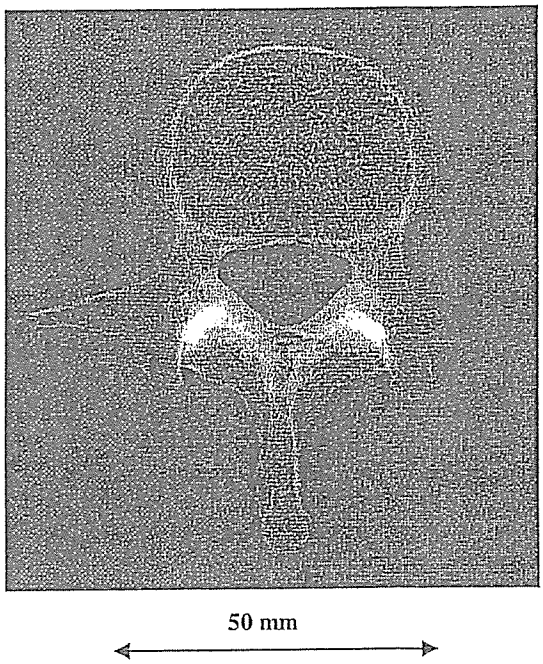

Fig. 8. Radiogram of a vertebra.

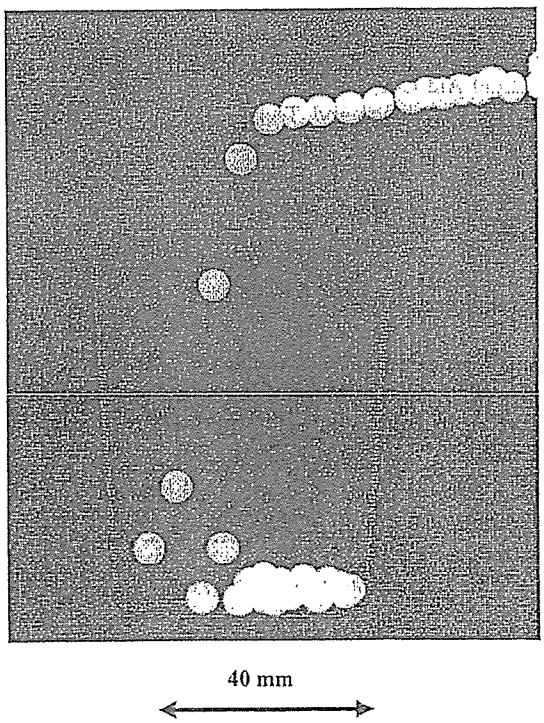

Fig. 9. Radiogram of plastic bullets falling into polypropylene beaker from a plastic test tube.

harmonic bremsstrahlung rays survived due to the X-ray resonation.

To perform monochromatic radiography, the higher harmonics are not necessary. Therefore, the condenser charging voltage should be minimized in order to decrease the intensities of higher harmonics, and the condenser capacity should be maximized to increase the characteristic X-ray intensity. On the other hand, because the intensities of harmonics increase with increases in the charging voltage, high-photon-energy monochromatic radiography may be realized.

In this research, we obtained sufficient characteristic X-ray intensity per pulse for CR radiography, and the generator produced number of characteristic K photons was approximately 1×10^8 photons/cm^2 at 1.0 m per pulse. In addition, since the photon energy of characteristic X-rays can be controlled by changing the target elements, various quasi-monochromatic high-speed radiographies, such as high-contrast angiography and mammography, will be possible.

Acknowledgments

This work was supported by Grants-in-Aid for Scientific Research (13470154, 13877114, 16591181, and 16591222) and Advanced Medical Scientific Research from MECSST, Health and Labor Sciences Research Grants (RAMT-nano-001, RHGTEFB-genome-005 and RHGTEFB-saisei-003), Grants from the Keiryo Research Foundation, the Promotion and Mutual Aid Corporation for Private Schools of Japan, the Japan Science and Technology Agency (JST), and the New Energy and Industrial Technology Development Organization (NEDO, Industrial Technology Research Grant Program in '03).

References

Ando, M., Maksimenko, M., Sugiyama, H., Pattanasiriwisawa, W., Hyodo, K., Uyama, C., 2002. A simple X-ray dark- and bright- field imaging using achromatic Laue optics. Jpn J. Appl. Phys. 41, L1016–L1018.

Davis, T.J., Gao, D., Gureyev, T.E., Stevenson, A.W., Wilkins, S.W., 1995. Phase-contrast imaging of weakly absorbing materials using hard X-rays. Nature 373, 595–597.

Germer, R., 1979. X-ray flash techniques. J. Phys. E: Sci. Instrum. 12, 336–350.

Hyodo, K., Ando, M., Oku, Y., Yamamoto, S., Takeda, T., Itai, Y., Ohtsuka, S., Sugishita, Y., Tada, J., 1998. Development of a two-dimensional imaging system for clinical applications of intravenous coronary angiography using intense synchrotron radiation produced by a multipole wiggler. J. Synchrotron. Rad. 5, 1123–1126.

Macchietto, C.D., Benware, B.R., Rocca, J.J., 1999. Generation of millijoule-level soft-X-ray laser pulses at a 4-Hz repetition rate in a highly saturated tabletop capillary discharge amplifier. Opt. Lett. 24, 1115–1117.

Momose, A., Takeda, T., Itai, Y., Hirano, K., 1996. Phase-contrast X-ray computed tomography for observing biological soft tissues. Nat. Med. 2, 473–475.

Mori, H., Hyodo, K., Tanaka, E., Mohammed, M.U., Yamakawa, A., Shinozaki, Y., Nakazawa, H., Tanaka, Y., Sekka, T., Iwata, Y., Honda, S., Umetani, K., Ueki, H., Yokoyama, T., Tanioka, K., Kubota, M., Hosaka, H., Ishizawa, N., Ando, M., 1996. Small-vessel radiography in situ with monochromatic synchrotoron radiation. Radiology 201, 173–177.

Rocca, J.J., Shlyaptsev, V., Tomasel, F.G., Cortazar, O.D., Hartshorn, D., Chilla, J.L.A., 1994. Demonstration of a discharge pumped table-top soft X-ray laser. Phys. Lev. Lett. 73, 2192–2195.

Rocca, J.J., Clark, D.P., Chilla, J.L.A., Shlyaptsev, V.N., 1996. Energy extraction and achievement of the saturation linit in a discharge-pumped table-top soft X-ray amplifier. Phys. Lev. Lett. 77, 1476–1479.

Sato, E., Kimura, S., Kawasaki, S., Isobe, H., Takahashi, K., Tamakawa, Y., Yanagisawa, T., 1990. Repetitive flash X-ray generator utilizing a simple diode with a new type of energy-selective function. Rev. Sci. Instrum. 61, 2343–2348.

Sato, E., Takahashi, K., Sagae, M., Kimura, S., Oizumi, T., Hayasi, Y., Tamakawa, Y., Yanagisawa, T., 1994a. Sub-kilohertz flash X-ray generator utilizing a glass-enclosed cold-cathode triode. Med. Biol. Eng. Comput. 32, 289–294.

Sato, E., Sagae, M., Takahashi, K., Shikoda, A., Oizumi, T., Hayasi, Y., Tamakawa, Y., Yanagisawa, T., 1994b. 10 kHz microsecond pulsed X-ray generator utilizing a hot-cathode triode with variable durations for biomedical radiography. Med. Biol. Eng. Comput. 32, 295–301.

Sato, E., Sato, K., Tamakawa, Y., 2000. Film-less computed radiography system for high-speed imaging. Ann. Rep. Iwate Med. Univ. Sch. Lib. Arts Sci. 35, 13–23.

Sato, E., Hayasi, Y., Germer, R., Tanaka, E., Mori, H., Kawai, T., Obara, H., Ichimaru, T., Takayama, K., Ido, H., 2003a. Irradiation of intense characteristic X-rays from weakly ionized linear molybdenum plasma. Jpn J. Med. Phys. 23, 123–131.

Sato, E., Hayasi, Y., Germer, R., Tanaka, E., Mori, H., Kawai, T., Ichimaru, T., Takayama, K., Ido, H., 2003b. Quasi-monochromatic flash X-ray generator utilizing weakly ionized linear copper plasma. Rev. Sci. Instrum. 74, 5236–5240.

Sato, E., Sagae, M., Tanaka, E., Hayasi, Y., Germer, R., Mori, H., Kawai, T., Ichimaru, T., Sato, S., Takayama, Y., Ido, H., 2004a. Quasi-monochromatic flash X-ray generator utilizing a disk-cathode molybdenum tube. Jpn J. Appl. Phys. 43, 7324–7328.

Sato, E., Hayasi, Y., Germer, R., Tanaka, E., Mori, H., Kawai, T., Ichimaru, T., Sato, S., Takayama, K., Ido, H., 2004b. Sharp characteristic X-ray irradiation from weakly ionized linear plasma. J. Electron. Spectrosc. Related Phenom. 137–140, 713–720.

Sato, E., Tanaka, E., Mori, H., Kawai, T., Ichimaru, T., Sato, S., Takayama, K., Ido, H., 2004c. Demonstration of

enhanced K-edge angiography using a cerium target X-ray generator. Med. Phys. 31, 3017–3021.

Sato, E., Tanaka, E., Mori, H., Kawai, T., Ichimaru, T., Sato, S., Takayama, Y., Ido, H., 2005a. Compact monochromatic flash X-ray generator utilizing a disk-cathode molybdenum tube. Med. Phys. 32, 49–54.

Sato, E., Tanaka, E., Mori, H., Kawai, T., Sato, S., Takayama, Y., 2005b. High-speed enhanced K-edge angiography utilizing cerium plasma X-ray generator. Opt. Eng. 44, 049001–049016.

Sato, E., Tanaka, E., Mori, H., Kawai, T., Sato, S., Takayama, Y., 2005c. Clean monochromatic X-ray irradiation from weakly ionized linear copper plasma. Opt. Eng. 44, 049002–049016.

Shikoda, A., Sato, E., Sagae, M., Oizumi, T., Tamakawa, Y., Yanagisawa, T., 1994. Repetitive flash X-ray generator having a high-durability diode driven by a two-cable-type line pulser. Rev. Sci. Instrum. 65, 850–856.

Takahashi, K., Sato, E., Sagae, M., Oizumi, T., Tamakawa, Y., Yanagisawa, T., 1994. Fundamental study on a long-duration flash X-ray generator with a surface-discharge triode. Jpn J. Appl. Phys. 33, 4146–4151.

Thompson, A.C., Zeman, H.D., Brown, G.S., Morrison, J., Reiser, P., Padmanabahn, V., Ong, L., Green, S., Giacomini, J., Gordon, H., Rubenstein, E., 1992. First operation of the medical research facility at the NSLS for coronary angiography. Rev. Sci. Instrum. 63, 625–628.

Available online at www.sciencedirect.com
ScienceDirect
Radiation Physics and Chemistry 75 (2006) 2008–2013
Radiation Physics and Chemistry
www.elsevier.com/locate/radphyschem

Tunable narrow-photon-energy X-ray generator utilizing a tungsten-target tube

Eiichi Sato[a,*], Hiroshi Sugiyama[b], Masami Ando[b], Etsuro Tanaka[c], Hidezo Mori[d], Toshiaki Kawai[e], Takashi Inoue[f], Akira Ogawa[f], Kazuyoshi Takayama[g], Jun Onagawa[h], Hideaki Ido[h]

[a]*Department of Physics, Iwate Medical University, 3-16-1 Honchodori, Morioka 020-0015, Japan*
[b]*Photon Factory, Institute of Materials Structure Science, High Energy Accelerator Research Organization, 1-1 Oho, Tsukuba 305-0801, Japan*
[c]*Department of Nutritional Science, Faculty of Applied Bio-science, Tokyo University of Agriculture, 1-1-1 Sakuragaoka, Setagaya-ku 156-8502, Japan*
[d]*Department of Cardiac Physiology, National Cardiovascular Center Research Institute, 5-7-1 Fujishirodai, Suita, Osaka 565-8565 Japan*
[e]*Electron Tube Division #2, Hamamatsu Photonics K.K., 314-5 Shimokanzo, Iwata 438-0193, Japan*
[f]*Department of Neurosurgery, School of Medicine, Iwate Medical University, 19-1 Uchimaru, Morioka 020-8505, Japan*
[g]*Shock Wave Research Center, Institute of Fluid Science, Tohoku University, 2-1-1 Katahira, Sendai 980-8577, Japan*
[h]*Department of Applied Physics and Informatics, Faculty of Engineering, Tohoku Gakuin University, 1-13-1 Chuo, Tagajo 985-8537, Japan*

Accepted 23 November 2005

Abstract

A preliminary experiment for producing narrow-photon-energy cone-beam X-rays using a silicon single crystal is described. In order to produce low-photon-energy X-rays, a 100-μm-focus X-ray generator in conjunction with a (1 1 1) plane silicon crystal is employed. The X-ray generator consists of a main controller and a unit with a high-voltage circuit and a microfocus X-ray tube. The maximum tube voltage and current were 35 kV and 0.50 mA, respectively, and the X-ray intensity of the microfocus generator was 48.3 μGy/s at 1.0 m from the source with a tube voltage of 30 kV and a current of 0.50 mA. The effective photon energy is determined by Bragg's angle, and the photon-energy width is regulated by the angle delta. Using this generator in conjunction with a computed radiography system, quasi-monochromatic radiography was performed using a cone beam with an effective energy of approximately 17 keV.

PACS: 87.59.–e; 87.59.Bh; 87.64.Gb

Keywords: Narrow-photon-energy X-rays; Tunable photon energy; Silicon single crystal; Cone beam

1. Introduction

Since the birth of the synchrotron, monochromatic parallel X-ray beams have been applied to X-ray phase-contrast radiography (Davis et al., 1995; Momose et al.,

*Corresponding author.
E-mail address: dresato@iwate-med.ac.jp (E. Sato).

0969-806X/$ - see front matter © 2006 Elsevier Ltd. All rights reserved.
doi:10.1016/j.radphyschem.2005.11.019

1996; Ando et al., 2002) and enhanced K-edge angiography (Thompson et al., 1992; Mori et al., 1996; Hyodo et al., 1998). The phase imaging is primarily based on the X-ray refraction, and the angiography is performed using X-rays with a photon energy of just beyond the K-absorption edge of iodine.

In order to perform high-speed medical radiography, although several different flash X-ray generators utilizing cold-cathode tubes have been developed (Sato et al., 1990, 1994a, b; Shikoda et al., 1994; Takahashi et al., 1994), quasi-monochromatic flash X-ray generators (Sato et al., 2003a, b, 2004a,b, 2005a–c) are useful to produce clean K-series characteristic X-rays without using a filter. Therefore, we have performed a demonstration of cone-beam K-edge angiography utilizing a cerium plasma generator, since K-series characteristic X-rays from the cerium target are absorbed effectively by iodine. In view of this situation, we have developed a steady state X-ray generator utilizing a cerium-target tube (Sato et al., 2004c), and have demonstrated enhanced K-edge angiography utilizing cerium Kα lines.

Without using synchrotrons, X-ray phase-contrast radiography for edge enhancement has been performed using a microfocus X-ray tube (Wilkins et al., 1996), and the digital imaging achieved with a 100-μm-focus molybdenum tube has been applied effectively to perform mammography (Ishisaka et al., 2000).

In this paper, we present a tunable narrow-photon-energy X-ray generator utilizing a single silicon crystal, and examine its suitability for energy-selective cone-beam radiography.

2. Experimental setup

Fig. 1 shows the block diagram of the X-ray generator, which consists of a main controller and an X-ray tube unit with a Cockcroft–Walton circuit and a 100-μm-focus X-ray tube. The tube voltage, the current, and the exposure time can be controlled by the controller. The main circuit for producing X-rays is illustrated in Fig. 2, and employed the Cockcroft–Walton circuit in order to decrease the dimensions of the tube unit. In the X-ray tube, positive and negative high voltages are applied to the anode and cathode electrodes, respectively. The filament heating current is supplied by an AC power supply in the controller in conjunction with an insulation transformer. The maximum tube voltage and current of the generator are 105 kV and 0.50 mA, respectively. In this experiment, the tube voltage applied was from 18 to 34 kV, and the tube current was 0.50 mA (maximum current) by the filament temperature. The exposure time is controlled in order to obtain optimum X-ray intensity.

The narrow-photon-energy X-ray generator utilizing a single silicon crystal of (1 1 1) plane is shown in Fig. 3. The effective photon energy is determined by Bragg's angle, and the photon-energy width is regulated by the

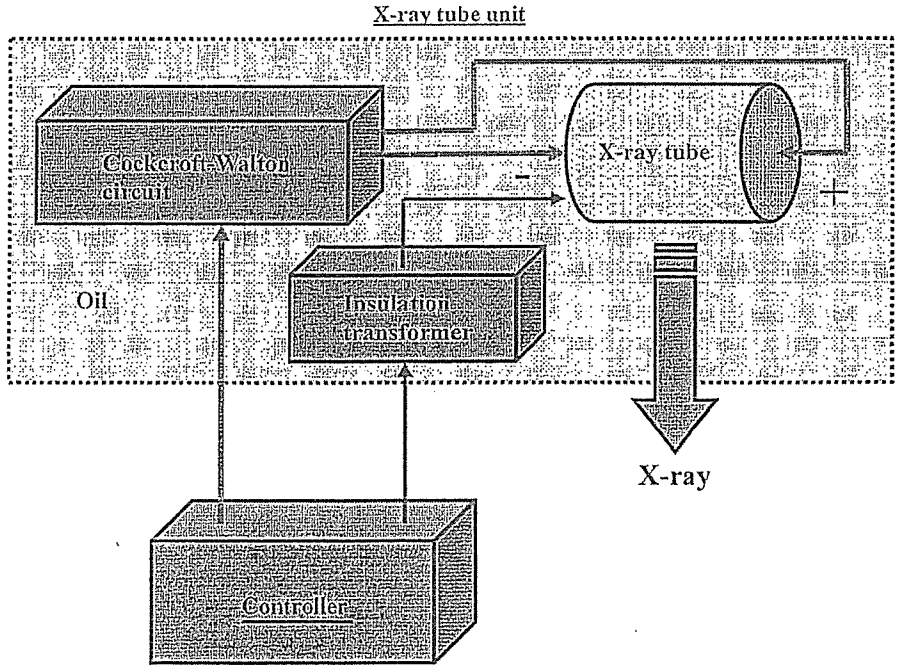

Fig. 1. Block diagram of a compact 100-μm focus X-ray generator with a tungsten-target radiation tube.

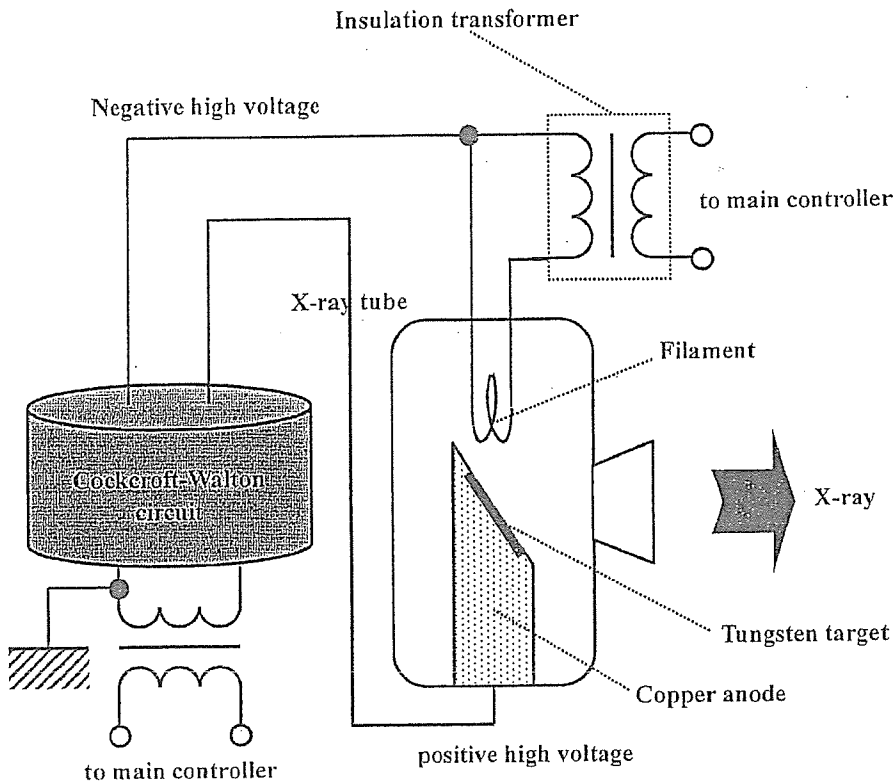

Fig. 2. Main circuit of the X-ray generator.

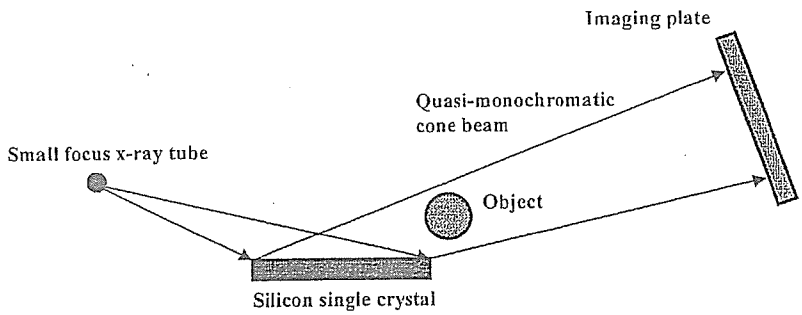

Fig. 3. Experimental setup of the narrow-photon-energy X-ray generator utilizing a single silicon crystal.

angle delta. Using this generator in conjunction with a computed radiography (CR) system (Sato et al., 2000), quasi-monochromatic radiography was performed using a cone beam with an effective energy of approximately 17 keV.

3. Results

3.1. X-ray intensity

X-ray intensity was measured by a Victoreen 660 ionization chamber at 1.0 m from the X-ray source (Fig. 4). At a constant tube current of 0.50 mA, the X-ray intensity increased when the tube voltage was increased. In this measurement, the intensity with a tube voltage of 30 kV was 48.3 μGy/s at 1.0 m from the source.

3.2. Radiography

The radiography was performed by the CR system (Konica Minolta Regius 150) with a sampling pitch of 87.5 μm, and the conditions for radiography were as in Fig. 3. Fig. 5 shows the irradiation field diffracted by the crystal with photon energies of approximately 17 keV.

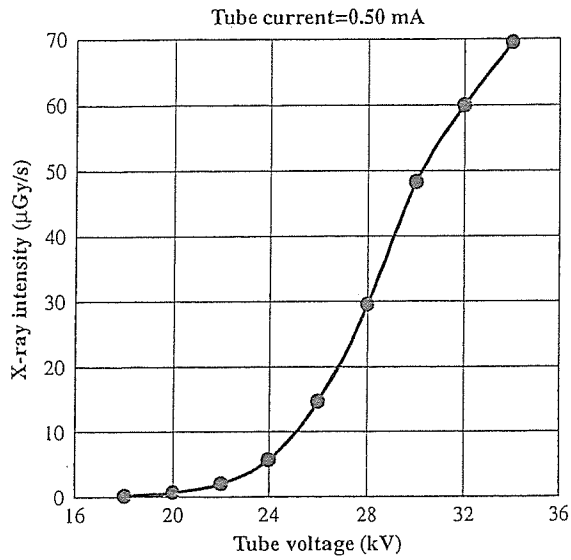

Fig. 4. X-ray intensity (μGy/s) as a function of tube voltage (kV) with a tube current of 0.50 mA.

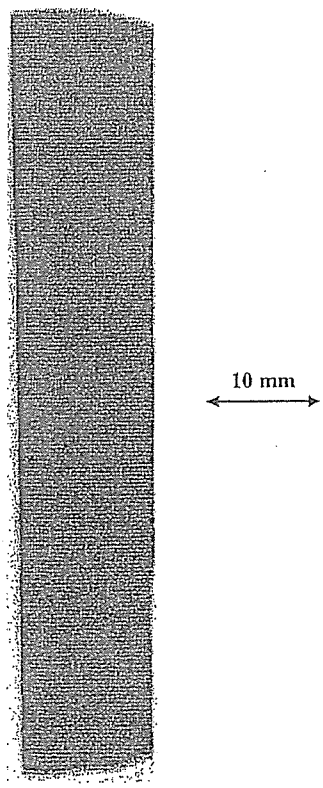

Fig. 5. Irradiation field with photon energies of approximately 17 keV measured using the CR system with a tube voltage of 30 kV.

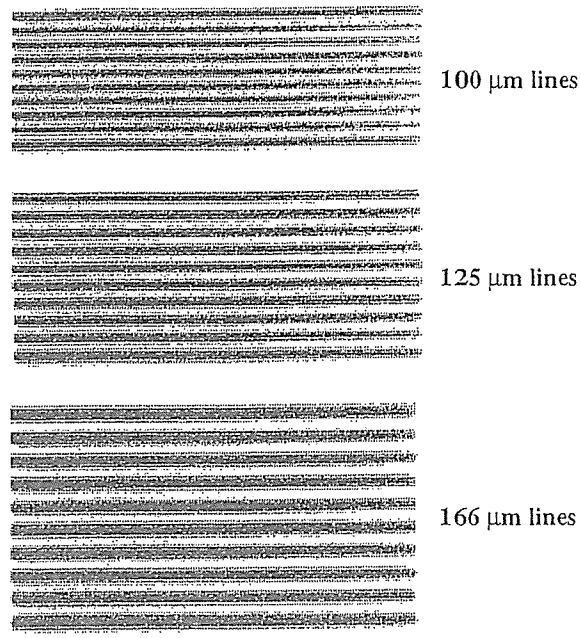

Fig. 6. Radiogram of a lead test chart for measuring the spatial resolution.

Because the width of the irradiation field was narrow due to the angle, the distance between the crystal and the imaging plate should be increased. Fig. 6 shows a radiogram of a test chart for determining the spatial resolution. In this radiography, 100-μm-wide lead lines (5 line pair) were observed. Subsequently, fine bone structures were visible in radiograms of a vertebra (Fig. 7), and fine blood vessels were observed in an angiogram of a rabbit heart (Fig. 8).

4. Conclusion and outlook

In summary, we employed a 100-μm-fosus X-ray generator with a tungsten-target tube and succeeded in producing narrow-photon-energy bremsstrahlung X-rays, which are refracted by a silicon single crystal of (1 1 1) plane. The photon energy width is primarily determined by the distance between the X-ray source and the crystal plate, and the irradiation field increases with increases in the distance between the crystal and the imaging plate. Because we employed the microfocus tube, phase-contrast effect was added in the radiography.

The microfocus generator produced maximum X-ray intensity was approximately 50 μGy/s at 1.0 m from the source, but the intensity was decreased substantially after the diffraction. Therefore, a high-current tungsten tube with a large focus should be employed in cases where the phase-contrast radiography is not employed.

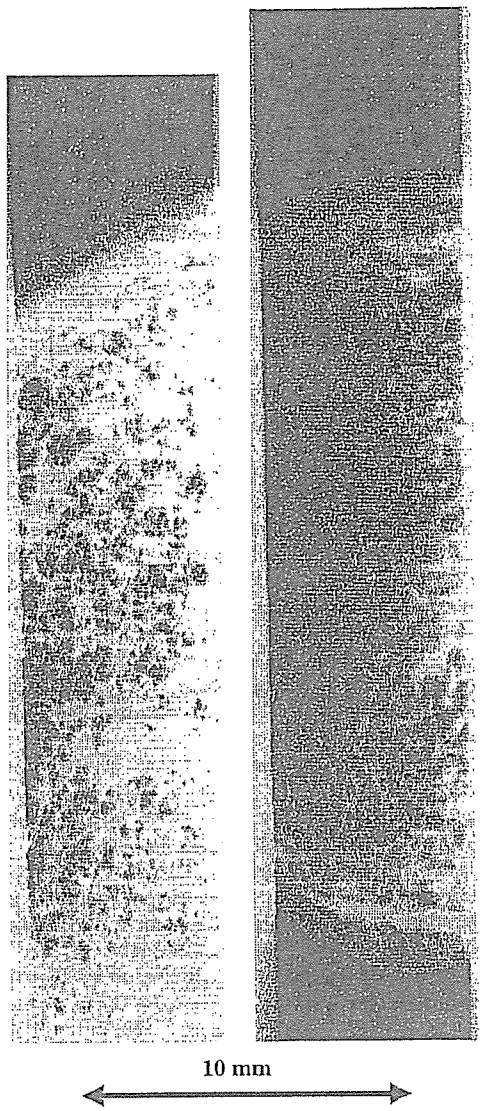

Fig. 7. Radiograms of a vertebra.

The magnification method is needed in phase-contrast radiography, and the method increases the spatial resolution of the digital radiography. Next, in conventional cohesion radiography, the spatial resolution is primarily determined by the sampling pitch of the CR system of 87.5 μm. Therefore, to improve the spatial resolution in cohesion radiography, the resolution of the CR system should be improved to approximately 50 μm (Konica Minolta Regius 190). In addition, the spatial resolution can be improved easily to approximately 50 μm or less in cases where an X-ray film is employed.

In this experiment, although we employed the (1 1 1) plane to perform soft radiography, other planes should be employed to perform high-photon-energy radiography. In conjunction with an analyzer crystal, this

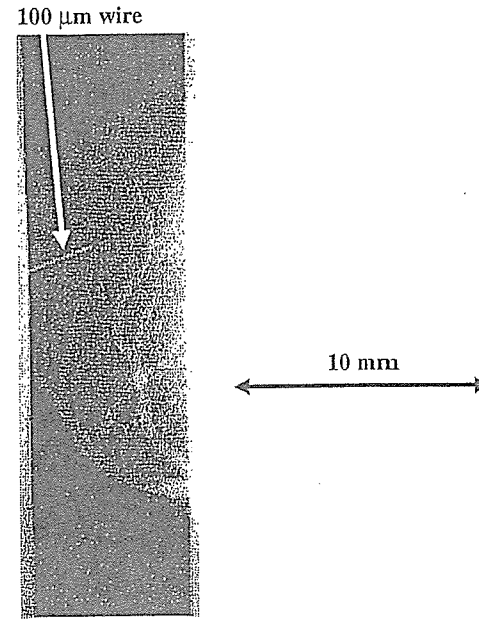

Fig. 8. Angiogram of a rabbit heart.

narrow-photon-energy cone-beam radiography using a microfocus X-ray tube could be useful for phase-contrast radiography as an alternative to radiography using synchrotrons.

Acknowledgments

This work was supported by Grants-in-Aid for Scientific Research (13470154, 13877114, 16591181, and 16591222) and Advanced Medical Scientific Research from MECSST, Health and Labor Sciences Research Grants (RAMT-nano-001, RHGTEFB-genome-005 and RHGTEFB-saisei-003), Grants from the Keiryo Research Foundation, the Promotion and Mutual Aid Corporation for Private Schools of Japan, the Japan Science and Technology Agency (JST), and the New Energy and Industrial Technology Development Organization (NEDO, Industrial Technology Research Grant Program in '03).

References

Ando, M., Maksimenko, M., Sugiyama, H., Pattanasiriwisawa, W., Hyodo, K., Uyama, C., 2002. A simple X-ray dark- and bright- field imaging using achromatic Laue optics. Jpn. J. Appl. Phys. 41, L1016–L1018.

Davis, T.J., Gao, D., Gureyev, T.E., Stevenson, A.W., Wilkins, S.W., 1995. Phase-contrast imagimg of weakly absorbing materials using hard X-rays. Nature 373, 595–597.